Synthesis and characterization of nickel boride nanoparticles for energy conversion catalyst materials – The effect of annealing temperature

Layla Haythoor Kharboot [a,b], Hui Xin Lim [a], Tuty Asma Abu Bakar [a,c],
Abdillah Sani Mohd Najib [a,c], Nur Safwati Mohd Nor [a], Norhuda Hidayah Nordin [d],
Nor Akmal Fadil [a,c]

[a] *Faculty of Mechanical Engineering, Universiti Teknologi Malaysia, 81310 Johor Bahru, Johor, Malaysia*
[b] *Wasit Water Directorate, Wasit governorate, Wasit, Iraq*
[c] *Material Research Consultancy Group, Universiti Teknologi Malaysia, 81310 Johor Bahru, Johor, Malaysia*
[d] *Department of Manufacturing and Materials Engineering, Kulliyyah of Engineering, International Islamic University Malaysia, Jalan Gombak, 53100 Kuala Lumpur, Malaysia*

ARTICLE INFO

ABSTRACT

In the recent technology development, fuel cell has been widely used in many applications, including transportation and industry. Platinum catalysts are used to catalyst the reaction at the oxygen electrode, but they are expensive and has limited supply. A nickel-boron nanoparticle catalyst is proposed as a substitute for fuel cell catalyst material. The objectives are to evaluate the effect of the annealing process and to determine the characteristics of the annealed nanoparticles using scanning electron microscopy - energy dispersive X-ray (SEM-EDS), inductively coupled plasma optical emission spectroscopy (ICP-OES) analysis, total organic carbon (TOC) analysis and X-ray diffraction (XRD). A wet chemical method was used to synthesize nickel-boron nanoparticles by chemical reduction (co-reduction) of nickel chloride and sodium borohydride. As-synthesized nickel-boron nanoparticles were annealed at temperatures of 200, 300, 400, 500, and 700 °C in an argon atmosphere for 2 h. From the experimental results, nickel-boron nanoparticles annealed at 300 °C with equal dispersion of crystalline Ni and crystalline Ni_3B showed the highest catalyst performance. The yield of nickel-boron nanoparticles sized 1.1364 nm was smaller than in the literature (37 nm). The size of Ni-B nanoparticles was calculated by using the Scherrer equation with the values of full width half maximum (FWHM) obtained by peak fitting following the Gaussian model. Smaller Ni-B nanoparticles have a higher surface-area-to-volume ratio, which increases the exposure of the active sites (crystalline Ni and crystalline Ni_3B phase) to the reactants (methanol) and improves catalytic activity.

1. Introduction

A particle is known as a nanoparticle when its size is in the nanoscale range [1]. Nanoparticles have a size range from 1 to 100 nm: they are undetectable by the naked eye. Nanoparticles exhibit new physical and chemical properties compared to bulk materials. They can be used in various applications, including medicine, aerospace, and catalysis. For instance, they effectively deliver drugs to the target site, resulting in increasing therapeutic benefits and minimizing the side effects [2]. In addition, nanoparticles are used as catalyst materials, and they can be classified into three categories for their use: homogeneous catalysts, heterogeneous catalysts, and photocatalysts. Recently, global energy consumption has increased steadily with the rapid development of

science and technology. This phenomenon results in high usage of non-renewable energy sources, such as fossil fuel. Soon, they will no longer be able to meet our population's needs for daily operations. By encountering this issue, scientists and researchers are strategizing to generate renewable energies through a fuel cell, using nano-precious metal-based nanoparticles as the catalyst, in the same way as a platinum catalyst. Nanoparticles, such as nickel boride, can be applied as energy conversion catalysts or electrocatalysts in fuel cells [3]. This has led to overcoming issues associated with other catalysts due to the substantial surface-to-volume ratio compared with bulk materials [4].

The study by Azman et al. [5] found that fossil fuel is the dominant energy source of oil producer countries like Malaysia and Iraq, and the rising trends of fuel prices in the market and anthropogenic climate
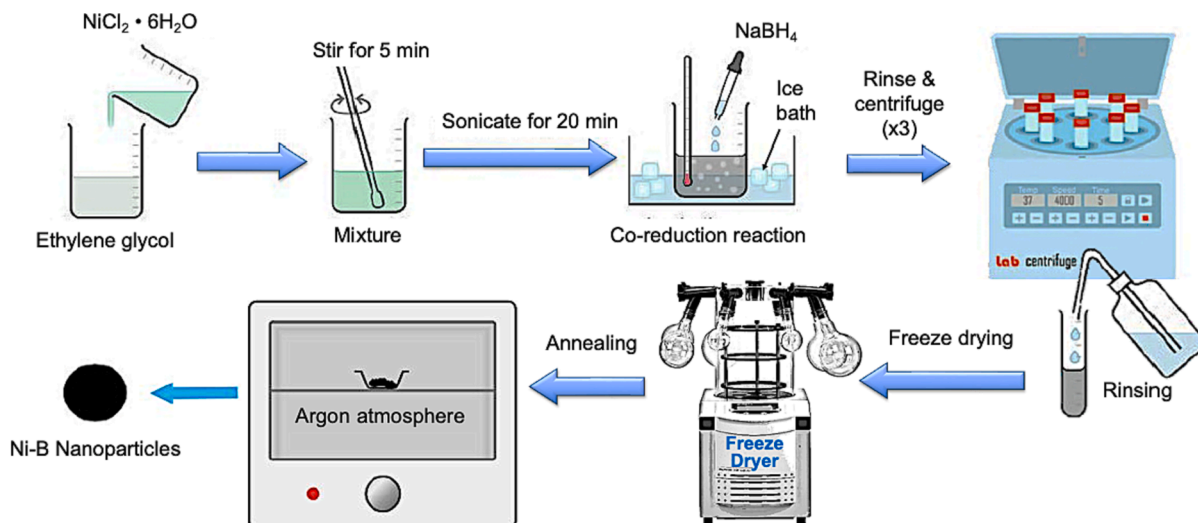
Fig. 1. Synthesis process of nickel boride nanoparticles.

change create a need for the development of renewable energy. The development of renewable energy sources is dependent on energy conversion and storage applications. There are two energy conversion system; namely, heat engines and fuel cells. An example of a heat engine is an internal combustion engine which it converts chemical energy from burning fossil fuels (gasoline or oil) into heat that ultimately drives a machince such as automobile [6]. The emission of a massive amount of greenhouse gases during the conversion causes negative effects on the environment. Although some fuel cell types still have obvious operational and environmental disadvantages that need to be addressed, fuel cells are less harmful to the environment than conventional energy conversion devices during operation [7]. As an example, for the fuel cell system of hydrogen fuel, the system relies on converting hydrogen and oxygen into water, yielding electricity and heat in the process. Though this is the most common method, methane and methanol can also be utilized for fuel cells due to their abundancy [4].

Platinum (Pt) nanoparticles are commonly used in fuel cells because they increase the reduction of oxygen to hydrogen peroxide. In theory, smaller Pt nanoparticles have lower binding energy for oxygenated species, leading to enhanced retention of *OOH toward oxygen reduction by the two-electron pathway reaction [8]. They are effective for speeding up the chemical reactions in hydrogen fuel cells. The advantage of using platinum nanoparticles is that they can withstand acidic conditions inside the cell. However, they are expensive and their availability are limted, make it demanding to ensure the sustainability fuel cells technology. Therefore, several studies have indicated that immense advancements have been accomplished in the performance and stability of non-platinum cathode catalysts during the past few years [9]. Thus, a non-precious metal-based catalysts specifically non-platinum catalyst, such as nickel, is suggested to replace the catalyst used in the fuel cell. Nickel is a very versatile material and has been utilized in many applications, including high-entropy materials [10], high-temperature applications [11], various electronic plating materials [12,13], solar absorbence agents [14] and catalysts [15]. They are available abundantly in nature and are low-cost compared to platinum catalysts and have high oxygen reduction reaction efficiency. They can absorb strongly enough to hold and activate the reactants optimally. Nickel catalysts have high catalytic performance and are applied in various types of fuel, such as sodium borohydride [15] and dry methane, reforming with the support of numerous metal oxides [16].

In the nano-catalysts structure, the crystallinity influences the catalytic performance of nanoparticles. This is proven by the study done by Li et al. [17] where the study determined the electrocatalytic behaviours and observed the electrocatalytic behaviours of both amorphous and crystalline Ni_3B by cyclic voltammetry (CV) and chronoamperometry (CA). They found that, the current density of crystalline Ni_3B has increased to 62 A g^{-1} at 0.55 V in 6 M KOH solution with 0.5 M methanol, demonstrating significant electrocatalytic activity performance. The strong methanol catalytic performance of the obtained crystalline Ni_3B is proven by the low onset potential and high anodic peak current density. In addition, the anodic current density increases with the increase of the methanol concentration. When methanol concentration reaches 0.5 M, the current density of crystalline Ni_3B approaches its maximum value of 64 A g^{-1}, whereas the current density of amorphous Ni_3B is only 46 A g^{-1}. It is evident that crystalline Ni_3B outperforms amorphous Ni_3B in electrocatalytic oxidation due to its high anodic peak current density. Additionally, the study aslo illustrated that the electrochemical stability of an electrocatalyst with crystalline and amorphous structure over a continuous 1200 s at a constant polarization potential of 0.55 V. For the crystalline Ni_3B, it is noted that there is a definite current decay from 77 Ag^{-1} to 65 A g^{-1} in the first few seconds, but there is almost no noticeable decay in the next 1200 s and the current density maintains at 76.6 % retention of the starting value, which is higher than that of the amorphous Ni_3B.

Motivated by the limitless opportunities offered by nickel particularly nickel-boron, this project is carried out to further explore the effect of annealing temperature on the nano-structure of nickel-boron nanoparticles to relate with their catalytic performance for methanol oxidation. We acknowledge that the as-synthesized nickel-boron nanoparticles have an amorphous structure which has limited capabilities as catalyst materials. However, the crystallinity of nickel-boron nanoparticles can be further improved and order the construction of nanoparticles, possibly increasing the nanoparticles' catalytic performance after undergoing a post-treatment process like annealing.

2. Methodology

This study focuses on the synthesis of nickel-boron nanoparticles by using the wet chemical method and anneal the synthesized nanoperticles for two hours at the temperature of 200, 300, 400, 500, and 700 °C. The as-synthesized and annealed nickel-boron nanoparticles were characterized through SEM-EDS, ICP-OES, TOC and XRD. The scope included analyzing the surface structure and morphology and detection of elemental composition through SEM-EDS; determining the elemental compostion of the nanoparticles by ICP-OES analysis, presence of carbon by TOC analysis, and phase analysis of nickel-boron nanoparticles annealed at various temperatures through XRD.
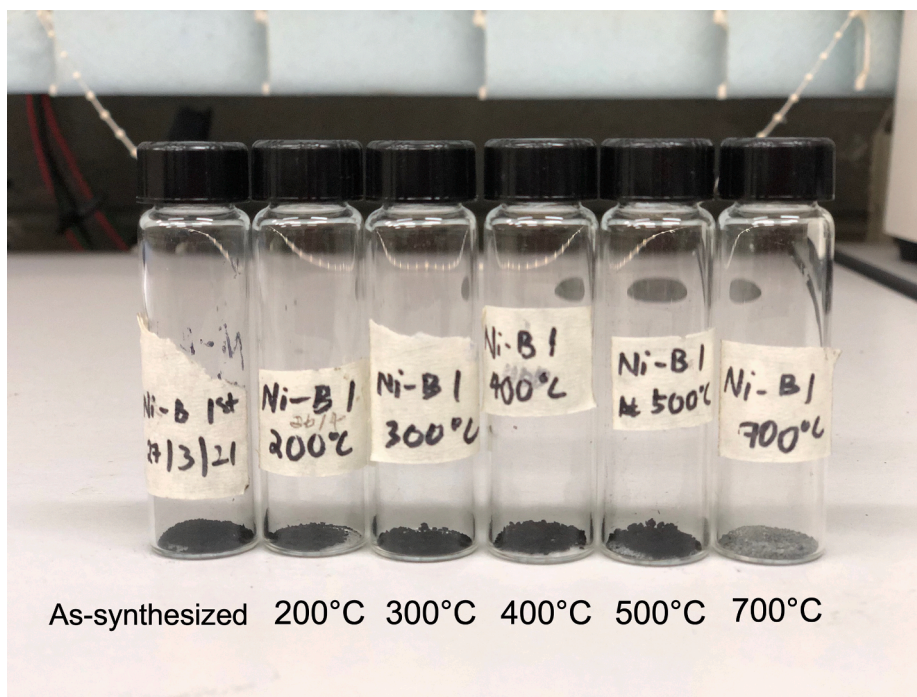
Fig. 2. The as synthesized and annealed samples up to 700 °C.

2.1. Synthesis of nickel boride nanoparticle

The wet chemical method was used to synthesize nickel boron nanoparticles, as illustrated in Fig. 1. This method can ease the process of controlling the surface area, grain size, and pore volume [18]. The synthesized method is adapted from Huang et al. [19] where the research had synthesized the nanoparticles through a nickel salt and sodium borohydride co-reduction reaction. The freeze-drying process was carried out after centrifuged-rinsed-centrifued for three times. The sample was freeze-dried overnight (24hrs) at the temperature of −55 °C using the freeze-drying machine (Alpha 1–2 LDplus) under vacuum conditions before annealing process in argon atmosphere.

2.2. Annealing process

Heat treatment can be used as the process of formation of active sites. It was conducted at various temperatures, that are 200, 300, 400, 500, and 700 °C in an argon atmosphere for 2 h. An argon atmosphere furnace (Nabertherm Muffle Furnace P330) was used for the annealing process of nanoparticles. The catalytic performance is expected to be improved after being heat treated by the annealing process. Fig. 2 shows the physical appearance of the as-synthesized and annealed nickel-boron nanoparticles with obvious changes in color for annealed nanoparticles at 700 °C. The change is suspected due to decomposition of nickel boride into nickel and boron at high temperature followed by the oxidation of both nickel and boron as proven by XRD analysis in the Section 3.3.

2.3. Characterization techniques of nickel boride nanoparticle

The as-synthesized nickel boride nanoparticles were characterized through various characterization methods. The scope includes the elemental analysis, phase and structure analysis, as well as surface morphology study. The scanning electron microscopy, SEM determined the surface morphology of material that had been synthesized 60 K magnification with a beam energy of 15.0 keV. Energy-dispersive X-ray (EDS) spectroscopy, coupled with a scanning electron microscope (SEM), was used to undertake an elemental study of as-synthesized and annealed nickel boride nanoparticles The instrument used for SEM-EDS was the Hitachi S-3400 N.

Inductively coupled plasma optical emission spectroscopy (ICP-OES) analysis was used for the determination of trace metals in the as-synthesised nickel-boron nanoparticles. The elemental metals to be calculated in the sample are nickel and boron. First, 0.05 g of the sample were weighed and 7 ml of HNO_3 were added. Then, the microwave digestion program proceeded, in which the mixture was microwaved at under 30 atm with power 90% for 30 min. 25 ml of the mixture were then added to a volumetric flask with ultra-pure water to the mark on the container. Further, a collection of calibrating solutions and sample solutions was mixed. Following these steps, the calculated element concentrations in the sample solution and the dilution factor of 200x were used to compute the concentrations in the original sample.

Total organic carbon, or TOC, is a unit of calculation used to specify how much carbon is present in an organic substance. The amount of inorganic carbon (IC), and organic carbon (OC) contained in the compound, as well as the overall amount of carbon (TC) present in the compound, were determined by the TOC analysis. All carbon sources were assumed to have been eliminated from the sample and identified for IC calculations.

The X-ray Diffraction (XRD) technique was used to identify the crystalline phases and orientation of the nanoparticles. XRD analyzed the composition pattern of the particle by the components, as each element has its unique peak in the spectrum. It observed the characteristics of the nanoparticles by using Bragg's law. X-ray diffraction (XRD) patterns of the nickel boride nanoparticle were obtained over a 2-theta range of 20–80° at a scan speed of 2.00° /min with a scan width of 0.02° on a Rigaku SmartLab X-ray diffractometer (Cu Ka, $\lambda = 1.54178$ Å) operated at 40 kV and 30 mA at room temperature. Following Bragg's equation, n = 2d sin θ, where n is an integer, is the wavelength of Cu K1 radiation, d is the interplanar spacing, and θ is the diffraction angle. Diffraction occurred from the sample of as-synthesized and annealed nickel boride nanoparticles.
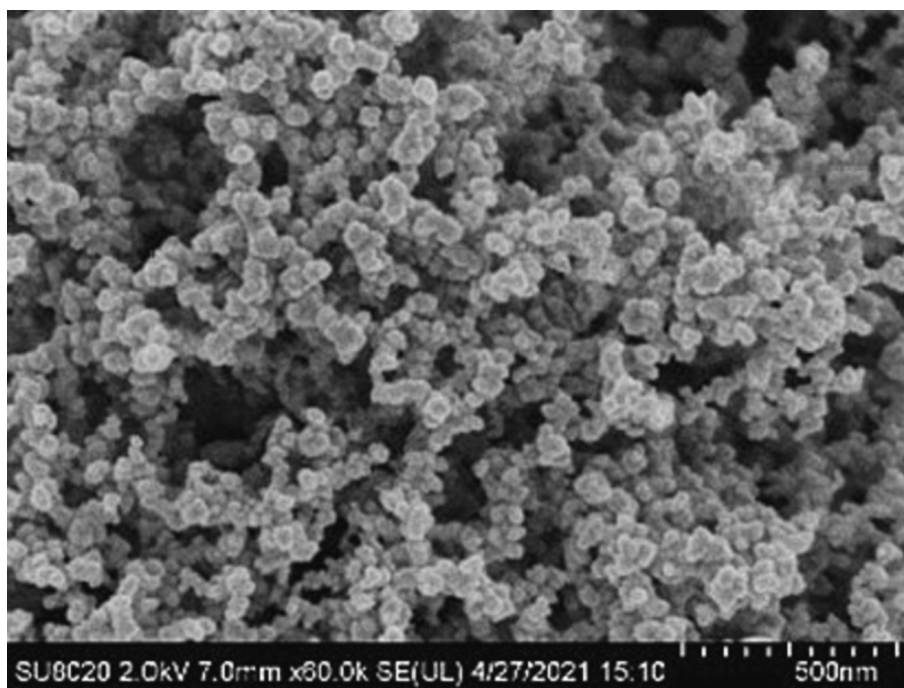
Fig. 3. SEM image of the as-synthesized Ni3B nanoparticles.

Table 1
Ni: B ratio for normalized atomic weightage of as-synthesized and annealed nickel boride nanoparticles.

Annealed Temperature (°C)	Norm. Atomic Weight Percentage (at%)		Ni: B Ratio
	Nickel (Ni)	Boron (B)	
0	40.03	59.97	0.67:1
200	40.45	59.55	0.68:1
300	29.80	70.20	0.42:1
400	29.16	70.84	0.41:1
500	25.88	74.12	0.35:1
700	29.73	70.27	0.42:1

3. Results and discussion

3.1. Elemental analysis.

3.1.1. Scanning electron microscopy - energy dispersive X-ray (SEM-EDS) analysis

From the SEM micrograph shown in Fig. 3, it is observed that there is uniform dispersion of spherical synthesized nickel-boron nanoparticles. From the micrograph, the as-synthesized nanoparticles are measured to be around 40 nm. The size is larger than the nickel-boron nanoparticles synthesized by Guo et al [16] where they calculated the nanoparticles using the Sherrer's equation of the XRD spectra. A comparison study on nanoparticles size is done using Sherrer's equation and is discussed in Section 3.3.

The EDX analysis by EDS equipped on the SEM was conducted to observe the elemental present in the nanoparticles and their composition. The elemental composition as well as calculated Ni:B ratio for

normalized atomic weightage of as-synthesized and annealed nickel boride nanoparticles is shown in Table 1. Overall, it is observed that the nickel composition drops drastically at the annealed temperature of 300 °C, while there is not much change when annealed at 200 °C as compared to as-synthesized samples. There has been a gradual decrease in the atomic percentage of nickel from 29.80 at% to 25.88 at% as the annealed temperature rises from 300 °C to 500 °C, followed by a slight rise to 29.73 at% at 700 °C. On the other hand, boron has an opposite trend to nickel, with the atomic weight percentage increasing from 59.97 at% to 74.12 at% as the annealed temperature increases from 0 to 500 °C and a slight drop to 70.27 at% at 700 °C. The reversal of the trend in atomic weights of nickel and boron at 700 °C might be caused by the chemical reaction of elemental present in the nanoparticles upon annealing. To investigate the reason why nickel composition is reduced with the increase of annealing temperature, phase analysis is conducted and discussed in Section 3.3.

3.1.2. Inductively coupled plasma optical emission spectroscopy (ICP-OES) analysis

ICP-OES analysis is used for the determination of trace elements in the as-synthesized nickel boride nanoparticles. The elements measured in the sample are nickel and boron. The concentration of nickel loaded in as-synthesized nickel boride nanoparticles was 1247 mg/L, while the concentration of boron loaded was 116.5 mg/L. Stoichiometric ratios of 66.24 at% and 33.66 at% were determined for nickel and boron in nickel boride nanoparticles as shown in Table 2.

3.1.3. Elemental analysis comparison study

By comparing the elemental composition measured by EDX and ICP-OES analysis for the as-synthesized nanoparticles shown in Table 1 and
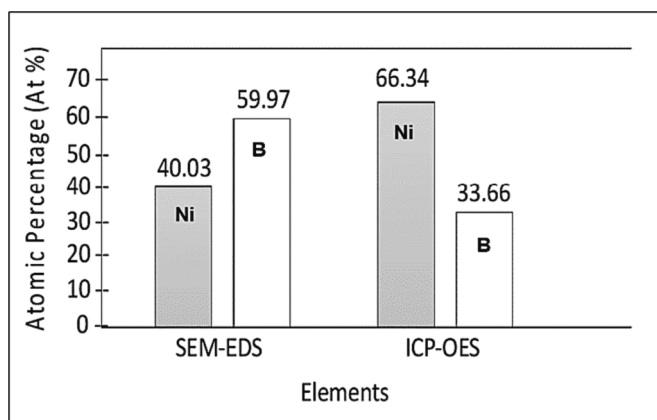
Table 2
Calculation of stoichiometric ratios for as-synthesized nickel-boron nanoparticles.

Analyte	Element	Molecular weight	Mean concentration (mg/L)	Molar Ratio	Atomic Percentage (at%)
Ni 231.604	Nickel	58.6934	1247	21.25	66.34
B 249.677	Boron	10.811	116.5	10.78	33.66

Fig. 4. Atomic percentages of Ni and B for SEM-EDS and ICP-OES analysis on the as-synthesized nickel-boron nanoparticles.

Table 2, both analyses proved the presence of nickel and boron in the as-synthesized nickel-boron nanoparticles. There was a significant variation in the percentages of nickel and boron for the SEM-EDS and ICP-OES, as shown in Fig. 4. Lower nickel fraction compared to boron is shown by the EDX analysis, but higher nickel fraction compared to boron is shown by ICP-OES. The working principle of the elemental analysis by EDX is a surface analysis, shows only part of the composition of the nanoparticles. The SEM-EDS approach helps detect elements on the surface of samples, but the ICP-OES method is particularly advantageous in determining the mineral content of entire volume of the samples. However, sample preparation in the SEM-EDS method is fast and easy, but for ICP-OES, in contrast, offers the advantage of lower detection limits with higher accuracy, even for the light elements. Given that each analysis has benefits and drawbacks, the best course of action is to evaluate the samples using both systems: first, a qualitative and quantitative overview using SEM-EDS, and then a precise quantification of the data using ICP-OES. Thus, the elemental composition obtained by ICP-OES analysis is more reliable than the SEM-EDS analysis. Therefore, it is proven that the synthesized nanoparticles have nickel-rich composition, and it is further verified by the XRD results discussed in Section 3.3.

3.2. Total organic carbon (TOC) analysis

The total organic carbon, or TOC, is a unit of calculation used to specify how much carbon is present in an organic substance. Since carbon content calculations are interconnected, total carbon content (TC), total inorganic carbon content (TIC), and total organic carbon content (TOC) are calculated by Eq. (1).

$$TC = TIC + TOC \tag{1}$$

According to the results, the average concentration of carbon is 7.917 ppm, with 0.7352 ppm of inorganic carbon and 7.182 ppm of organic carbon. As a result, the amount of inorganic carbon present in nickel boride nanoparticles is extremely low and is approximately equivalent to 0.7352 mg/L. It may be concluded that there is no detectable carbon in the nickel boride nanoparticle by contrasting it to the concentrations of nickel and boron in the ICP-OES experiment, which are 1247 mg/L and 116.5 mg/L, respectively. The presence of carbon in the nickel may results in the formation of Ni_3C, which may hinder the performance of nickel-boron catalytic performance. The presence of the Ni_3C structure is further verified by the phase analysis by XRD as discussed in Section 3.3.

3.3. Phase analysis by using X-ray powder diffraction (XRD)

Phase analysis of the as-synthesized and annealed nickel-boron

nanoparticles was conducted by XRD analysis as shown in Fig. 5. It can be observed that the as-synthesized and annealed samples up to 400 °C had an amorphous structure, indicating the nanoparticle size is small, as can be seen by the broad peaks of the XRD spectras. The broad peaks are close to the XRD patterns of Ni_2B and Ni_3B phases. The XRD peaks correspond to the (2 0 0), (0 3 1) and (3 1 1) planes of the Ni_3B phase at $2\theta = 34.32°$, $46.01°$, and $58.68°$, respectively, are the most dominant peaks that can be observed. Meanwhile, the peaks at $25.21°$ and $35.95°$ correspond to the (1 1 0) and (2 0 0) planes of the Ni_2B phase respectively. It can be observed that the peak intensity of XRD spectra corresponding to Ni_2B and Ni_3B increased with the increase of annealing temperature.

The increase in the peak intensity indicates that the nickel-boron nanoparticle size increases with the annealing temperature. The XRD spectra of annealed samples, however, showed a very broad peak corresponding to the (0 3 1) plane at $2\theta = 46.01°$, which possibly overlapped with other highest intensity peaks corresponding to the Ni_2B phase (plane (2 1 1) at $45.89°$). Furthermore, the XRD peaks for samples annealed at 300 °C showed a very broad peak corresponding to the (0 3 1) plane of the Ni_3B phase. At the annealing temperature of 500 °C, the diffraction peaks of Ni_3B are unseen, while diffraction peaks for Ni and NiO are visible. The presence of the FCC Ni phase matches the highest intensity of the (1 1 1) lattice plane as it is observed at $2\theta = 44.82°$ together with other peaks belong to FCC Ni and NiO. This indicates that an annealing temperature of 500 °C is high enough to decompose the nickel-boron metallic phase into its pure metallic form (FCC Ni), and subsequently allow the nickel oxide (NiO) reaction. A further increase of annealing temperature completely transformed the pure Ni into NiO, and allowed the growth of crystalline size of NiO at sufficiently high temperature. The high intensity peaks corresponding to crystalline NiO are assigned to the (1 1 1), (2 0 0), and (2 2 0) planes at $2\theta = 37.03°$, $43.02°$ and $62.48°$. It can be concluded that the crystalline Ni_3B is decomposed into pure nickel and starts to react with oxygen to form nickel oxide at 500 °C of annealing temperature, while 700 °C of annealing temperature is the limit for Ni to fully oxidize into NiO. Meanwhile, the XRD results have proved that no Ni_3C phase was observed in the samples, indicating that the synthesized Ni-B nanoparticles are clean from carbon inclusion that could possibly introduced by solvents and other by-products.

By comparing the EDX and XRD results, it is observed that the higher annealing temperatures produced marked phase changes, by forming various compositions. Fig. 6 shows the schematic diagram on how nanostructure of synthesized nickel-boron nanoparticles has changed by the annealing temperature. At the annealing temperature of 200 °C, the crystalline Ni_2B and Ni_3B nanoparticles are formed [20,21], while at 500 °C, some of the Ni_2B and Ni_3B nanoparticles decomposed into nickel and boron [22] to allow the formation of nickel oxide, where the oxygen is suspected come from the contamination in the argon environment. Finally, at 700 °C the Ni, which partly decomposed from nickel-boron nanoparticles is fully oxidized to form NiO. Besides, at 700 °C, boron oxide is formed on the surface of nanoparticles. However, due to the very thin layer of boron oxide and the limited penetration of X-ray detection of the XRD, the boron oxide phase is not able to be detected by XRD, as well as part of remined Ni_2B and Ni_3B nanoparticles [23]. Thus, it is expected that the multiple phases of crystalline Ni, Ni_2B, and Ni_3B can be obtained at the annealing temperature of 300 °C – 500 °C.

3.4. Particle size calculation

Based on the XRD spectra of as-synthesized samples and annealed samples shown in Fig. 7, peak analysis was conducted to determine the particle size of nanoparticles using Scherrer's equation. However, the peaks are too broad and include more than one individual peak. Therefore, peak convolution was performed to accurately determine the full width half maximum (FWHM) value by peak fitting following the Gaussian model. Scherrer's equation can be written as shown in
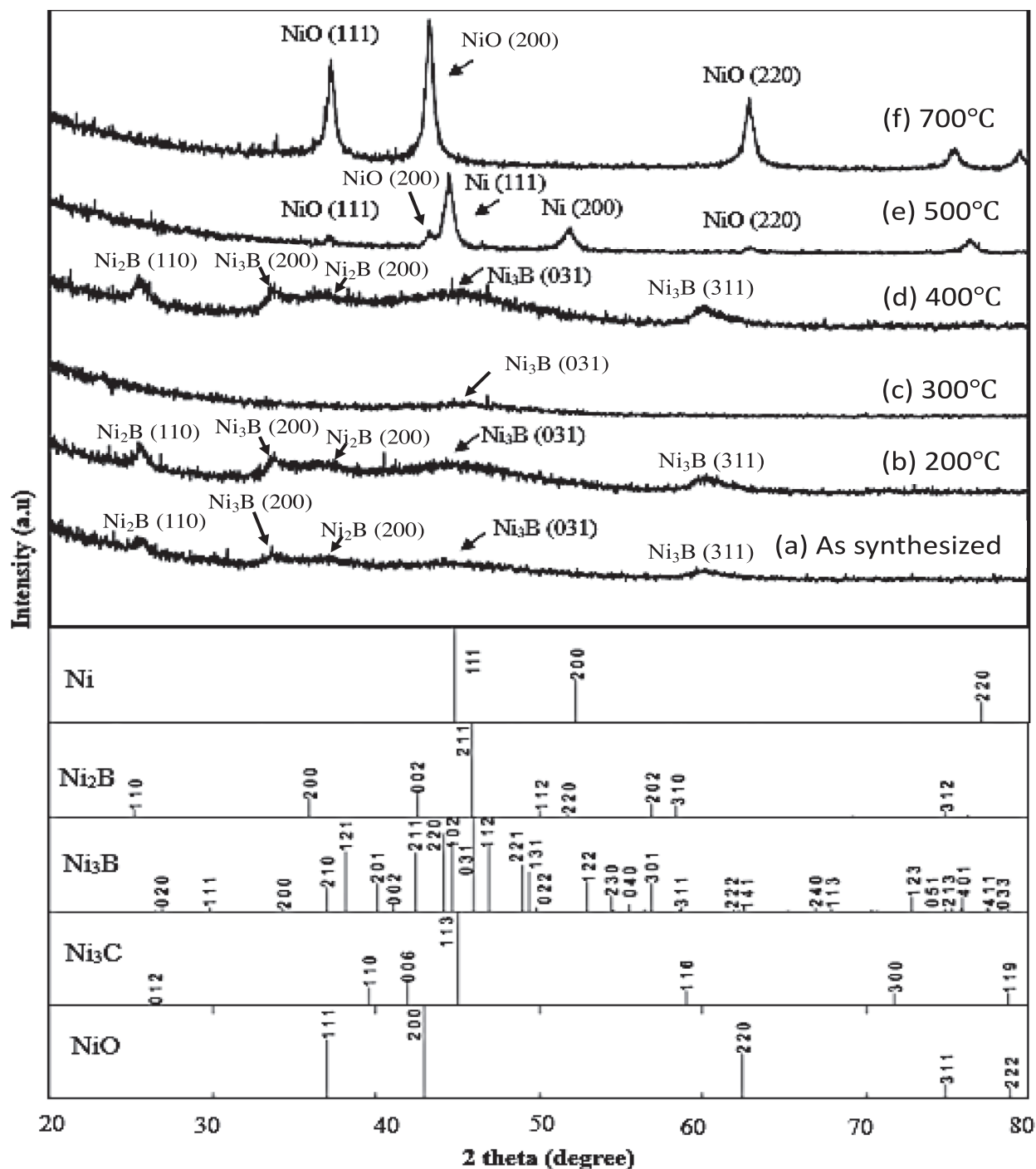
Fig. 5. XRD Spectra of as synthesized and annealed Ni-B nanoparticles at temperatures of 200 °C, 300 °C, 400 °C, 500 °C, and 700 °C.

Equation (2)

$$D = \frac{k\lambda}{\beta\cos\theta} \qquad (2)$$

where D is the mean size of the particle, K is a dimensionless shape factor, with a typical value of about 0.9, λ is the X-ray wavelength (Cu Ka = 1.54178 Å), β is the line broadening at half the maximum intensity (FWHM), after subtracting the instrumental line broadening, in radians, and θ is the Bragg angle.

Fig. 7 shows the convoluted peak of as-synthesized and annealed Ni-B samples at 200 °C and 400 °C. The FWHM values were determined on the convoluted peaks that correspond to the (2 0 0), (0 3 1) and (3 1 1)

planes of the Ni$_3$B phase. Table 3 shows the particle size of the Ni-B nanoparticles calculated using Scherrer's equation. The results show that the overall size of the Ni-B nanoparticles increased as the annealing temperature increased. A similar trend is observed by all peaks, in that as the annealing temperature rises, the diffraction peak also rises. The formation of sharp, narrow peaks results in lower FWHM values. Peaks becoming narrower are also a sign that the size of the nickel-boron nanoparticles is growing. Further evidence that the sample size is growing is provided by the fact that the intensities of the Bragg peaks of annealed nickel-boron samples are sharp and narrow as compared.

to as-synthesized nickel-boron nanoparticles. For all peak analyses of Ni$_3$B at the (2 0 0), (0 3 1) and (3 1 1) planes, it can be concluded that the
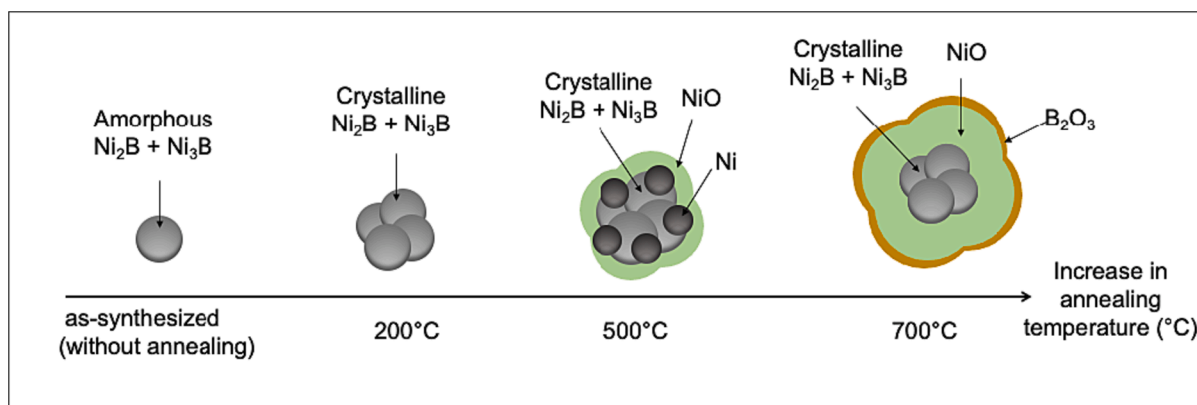
Fig. 6. The effect of annealing temperatures on the nano-structure of Ni-B nanoparticles.
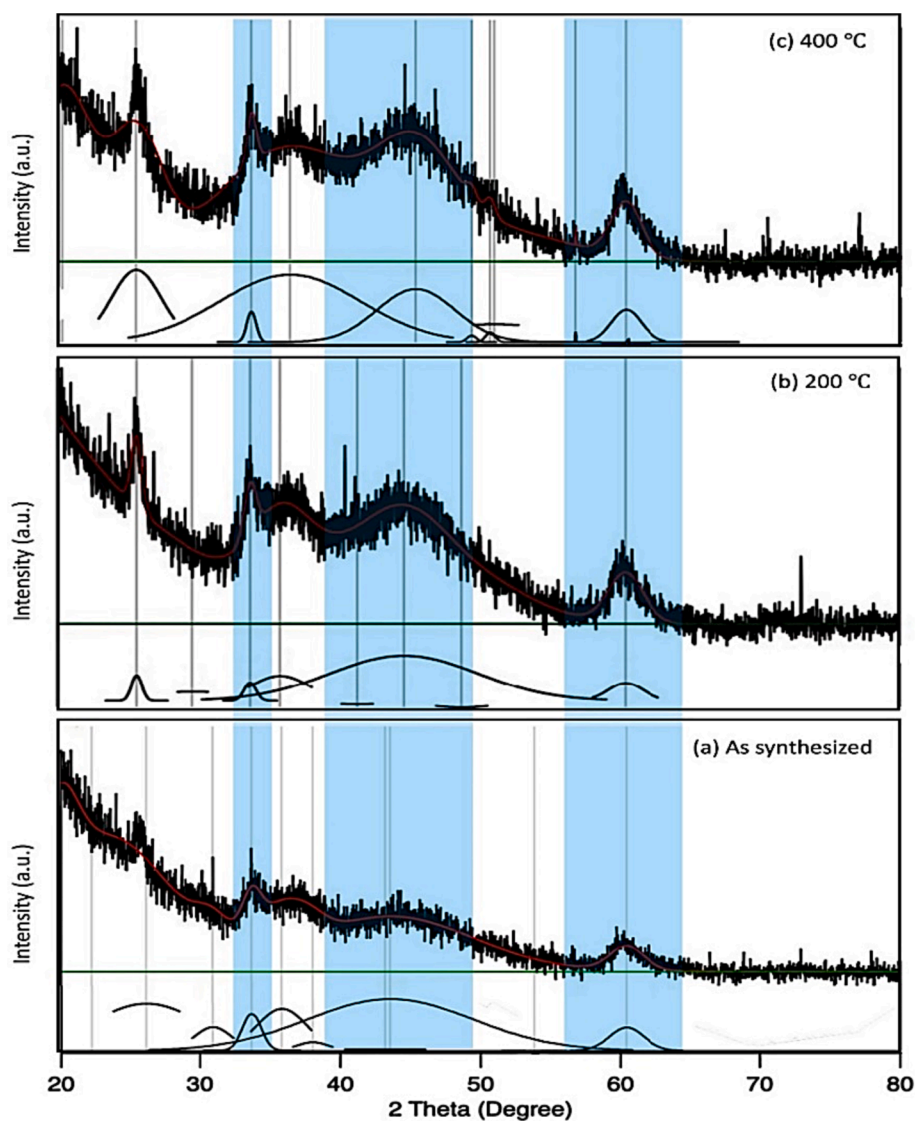

Fig. 7. Peak deconvolution of as-synthesized and annealed Ni-B nanoparticle samples at 200 °C and 400 °C for particle size calculation.

nanoparticle size of the as-synthesized sample is less than 1 nm.

When comparing the size of as-synthesized and annealed Ni-B nanoparticles in this study with similar reported work by Guo et al. (2016) [16], the Ni-B nanoparticles size of this study are much smaller, as shown in Fig. 8. Thus, they offer better catalytic performance as they have a larger surface area-to-volume ratio, increasing the exposure of active sites (crystalline Ni, Ni_2B, and Ni_3B phase) to the reactants (methanol) when annealed at temperature between 300 °C−500 °C.

Table 3
Particle size of Ni-B nanoparticles calculated using Scherrer's equation.

Peak list	Temperature (°C)	2 Theta	FWHM	Size (nm)
Ni₃B (200)	As synthesized	33.66	1.5906	5.7021
	200	33.75	1.0054	9.0193
	400	33.77	0.79342	11.4285
Ni₃B (031)	As synthesized	43.54	13.882	0.6391
	200	44.7	12.379	0.7148
	400	45.47	6.5444	1.3497
Ni₃B (311)	As synthesized	60.41	2.9128	2.9371
	200	60.47	2.9815	2.869
	400	60.43	2.566	3.3339

3.5. Catalytic performance of nickel boride nanoparticles for methanol oxidation.

3.5.1. Mechanism of nickel boride nanoparticles for methanol oxidation

In contrast to noble metals, the catalytic activity of non-precious, nickel-based electrocatalysts for alcohol oxidation is primarily related to the potential formation of an NiOOH active layer on the surface. The oxidation process of methanol starts at a potential value corresponds to the formation of NiOOH on the nickel-boron nanoparticles active surface. The reactions on the active layer cause methanol electro-oxidation to take place. It has been widely documented that methanol is oxidized on nickel-based catalysts at the potential at which nickel oxyhydroxide (NiOOH) is formed. Nickel hydroxide (Ni(OH)$_2$) converts into NiOOH during the oxidation of alcohols. NiOOH is believed to be a strong oxidant while also being reduced to Ni(OH)$_2$ by the Equation (3). Meanwhile, the amount of NiOOH on the Ni electrode surface is decreased by the oxidation of alcohols. The formation of NiOOH on the catalyst surface is accountable for the catalytic activity of methanol oxidation. Unlike noble metals, nickel-based non-precious electro-catalysts for alcohol oxidation have a higher potential for the formation of an NiOOH active layer on the surface, which is mainly responsible for their higher catalytic activity. The mechanism of nickel-boron nanoparticles for methanol oxidation is illustrated by Fig. 9.

$$\text{NiOOH} + \text{H}_2\text{O} + \text{e-} \rightarrow \text{Ni(OH)}_2 + \text{OH}^- \tag{3}$$

3.5.2. Crystallinity and effect of annealing temperatures on the catalytic activity of methanol oxidation

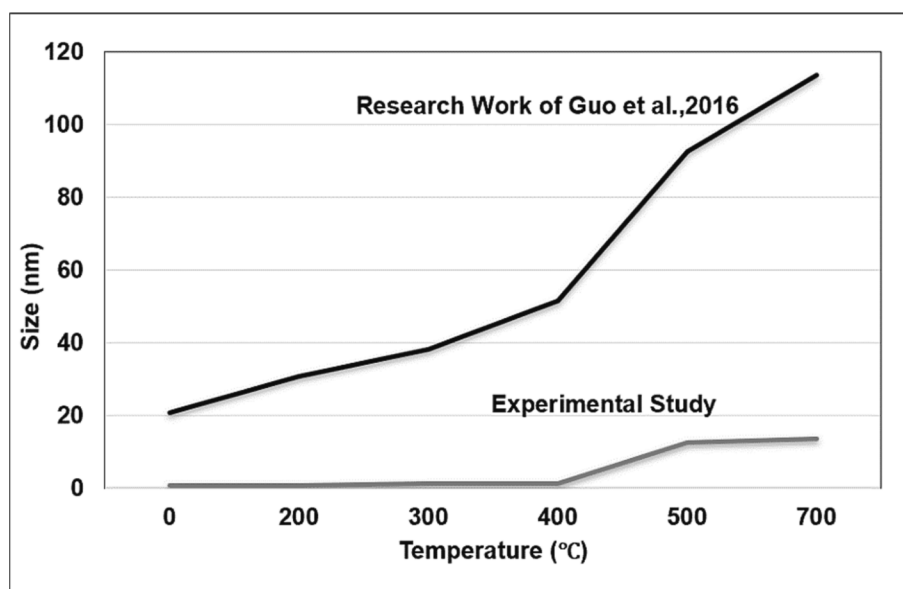Based on the previous study, the annealing process enhanced the

Fig. 8. Size distribution of Ni-B nanoparticles for the experimental work and research work of Guo et al. [16].
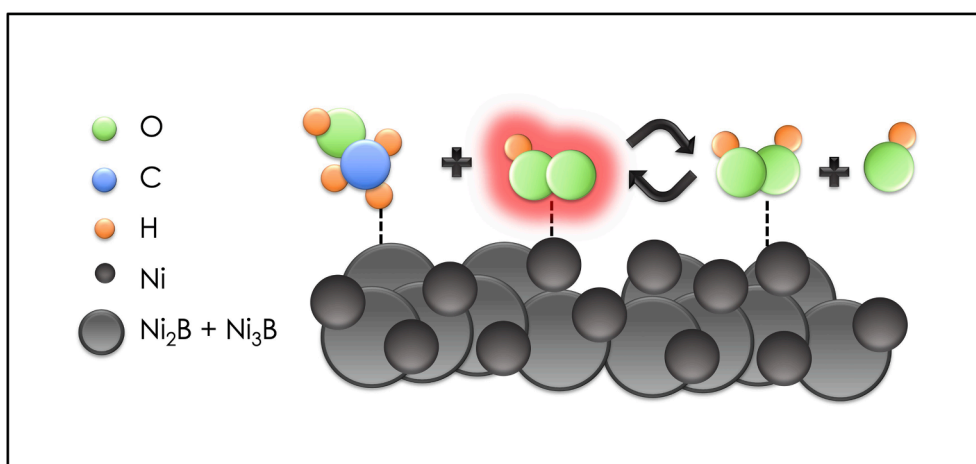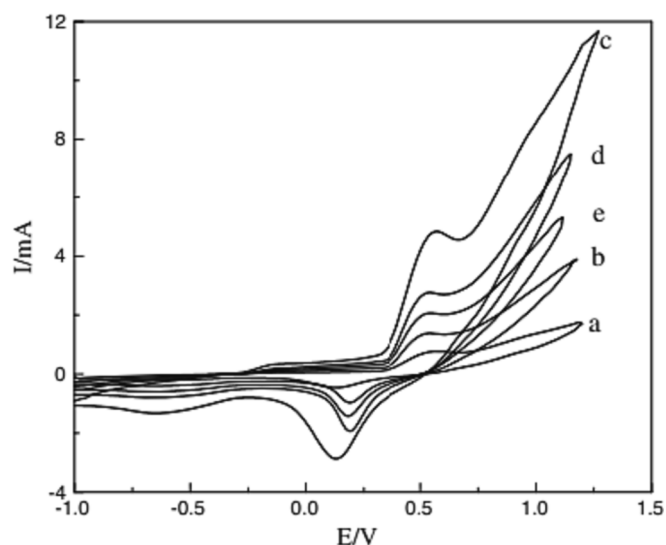
Fig. 9. Mechanism of nickel boride nanoparticles catalytic reaction for methanol oxidation.

Fig. 10. Cyclic voltammetry curve of (a) amorphous nickel-boron sample and nickel-boron samples annealed at (b) 280 °C, (c) 300 °C, (d) 340 °C, (e) 380 °C is plotted that subjected to methanol oxidation [16].

catalytic performance of nickel-boron nanoparticles as shown by the cyclic voltammetry curve for nickel-boron nanoparticles annealed at various temperatures in Fig. 10 [16]. Based on the curve, the highest anodic peak can be observed at the annealing temperature of 300 °C, that results in the best catalytic performance among the amorphous and varied annealed temperatures of the sample. In contrast, when nickel-boron and nickel boride are annealed at 280 °C, the anodic peak is still greater peaks and better catalytic performance compared to amorphous nickel-boron nanoparticles. Due to the dispersion of crystalline Ni and crystalline Ni_3B in the sample, an annealing temperature of 300 °C has the best catalytic performance for methanol oxidation. This is supported by the XRD examination, which shows that annealing nickel-boron at 300 °C results in a composition percentage of 59% Ni and 41% crystalline Ni_3B. The study also introduced a synergetic mechanism of methanol oxidation of annealed nickel-boron at 300 °C, where crystalline Ni is involved in the formation of NiOOH, while crystalline Ni_3B provides an adsorption surface to absorb methanol to quicken the oxidation reaction between NiOOH and methanol to form $Ni(OH)_2$ [16].

4. Conclusion

From the analysis of the results of this experimental work, it can be concluded that nickel-boron nanoparticles with equal dispersion of crystalline Ni and crystalline Ni_3B in the sample that was annealed at 300 °C had the highest catalytic performance among as-synthesized samples and samples annealed at temperatures of 200 °C, 300 °C, 400 °C, 500 °C, and 700 °C. This is because nickel-boron nanoparticles annealed at 300 °C has a stronger anodic peak and greater catalytic efficacy than amorphous and annealed nickel-boron nanoparticles at other annealing temperatures. Additionally, the nickel-boron nanoparticle size obtained in this experimental work was smaller than in previous research. The as-synthesized nickel-boron nanoparticle size (1.1364 nm) was smaller than in the literature (37 nm), as calculated by the Scherrer equation, with the values of full width half maximum (FWHM) obtained by peak fitting following the Gaussian model. Smaller Ni-B nanoparticles have a higher surface-area-to-volume ratio, which increases the exposure of the active sites (crystalline Ni and crystalline Ni_3B phase) to the reactant (methanol) and improves catalytic activity. The future study contains preparing new samples for photometric analysis.

Declaration of Competing Interest

The authors declare that they have no known competing financial interests or personal relationships that could have appeared to influence the work reported in this paper.

Data availability

Data will be made available on request.

References

[1] F. Trotta, A. Mele, Nanosponges Synthesis and Applications, John Wiley & Sons, 2019.

[2] J.K. Saucier-Sawyer, et al., Systemic delivery of blood-brain barrier-targeted polymeric nanoparticles enhances delivery to brain tissue, J. Drug Targeting 23 (2015) 736–749, https://doi.org/10.3109/1061186X.2015.1065833.

[3] I. Khan, K. Saeed, I. Khan, Nanoparticles: Properties, applications and toxicities, Arab. J. Chem. 12 (2019) 908–931, https://doi.org/10.1016/j.arabjc.2017.05.011.

[4] A.K. Hussein, Applications of nanotechnology in renewable energies - A comprehensive overview and understanding, Renew. Sustain. Energy Rev. 42 (2015) 460–476, https://doi.org/10.1016/j.rser.2014.10.027.

[5] A.Y. Azman, A.A. Rahman, N.A. Bakar, F. Hanaffi, A. Khamis. Study of renewable energy potential in Malaysia, in: 2011 IEEE 1st Conf. Clean Energy Technol. CET 2011 170–6. doi:10.1109/CET.2011.6041458.

[6] Y. Ge, L. Chen, F. Sun, Progress in finite time thermodynamic studies for internal combustion engine cycles, Entropy 18 (2016), https://doi.org/10.3390/e18040139.

[7] A. Haxhiu, A. Abdelhakim, S. Kanerva, J. Bogen, Electric power integration schemes of the hybrid fuel cells and batteries-fed marine vessels - An Overview, IEEE Trans. Transp. Electrif. 8 (2022) 1885–1905, https://doi.org/10.1109/TTE.2021.3126100.

[8] K. Jiang, J. Zhao, H. Wang, Catalyst design for electrochemical oxygen reduction toward hydrogen peroxide, Adv. Funct. Mater. 30 (2020) 1–11, https://doi.org/10.1002/adfm.202003321.

[9] N.A. Karim, S.K. Kamarudin, An overview on non-platinum cathode catalysts for direct methanol fuel cell, Appl. Energy 103 (2013) 212–220, https://doi.org/10.1016/j.apenergy.2012.09.031.

[10] N.H.A. Hassan, N.A. Fadil, N.F. Ibrahim, M.S. Jami, N.H. Nordin, High entropy alloy as catalyst for degradation of azo dye in Fenton process, AIP Conf. Proc. 2454 (2022), 060052, https://doi.org/10.1063/5.0079480.

[11] T. Dippong, E.A. Levei, O. Cadar, Recent advances in synthesis and applications of MFe_2O_4 (M= Co, Cu, Mn, Ni, Zn) nanoparticles, Nanomaterials 11 (6) (2021) 1560, https://doi.org/10.3390/nano11061560.

[12] N.L.M. Amin, S.Z. Yusof, M.N.A. Kahar, T.A.A. Bakar, N.A. Fadil, in: Tin Whiskers Formation and Growth on Immersion Sn Surface Finish under External Stresses by Bending, IOP Publishing, 2017, p. 012001, https://doi.org/10.1088/1757-899X/238/1/012001.

[13] N.A. Fadil, S.Z. Yusof, T.A. Abu Bakar, H. Ghazali, M.A. Mat Yajid, S.A. Osman, A. Ourdjini, Tin Whiskers' behavior under stress load and the mitigation method for immersion tin surface finish, Materials 14 (22) (2021) 6817, https://doi.org/10.3390/ma14226817.

[14] N.N.A. Azli, N.M. Amin, S.T. Oluhende, S.N.A. Mohamad, N.A. Fadil, Electroless deposited black nickel-phosphorous solar absorber coatings on carbon steel: effect of plating bath pH, Mater. Today: Proc. 39 (2021) 1071–1076, https://doi.org/10.1016/j.matpr.2020.06.087.

[15] N.A. Fadil, et al., Synthesis and electrocatalytic performance of atomically ordered nickel carbide (Ni_3C) nanoparticles, Chem. Commun. 50 (49) (2014) 6451–6453, https://doi.org/10.1039/x0xx00000x.

[16] J. Guo, Y. Hou, B. Li, Y. Wang, Ni_3B–Ni nanocomposites for improved electrocatalytic activity in methanol oxidation reaction, J. Appl. Electrochem. 46 (12) (2016) 1177–1186, https://doi.org/10.1007/s10800-016-1000-y.

[17] J. Li, et al., Crystalline nickel boride nanoparticle agglomerates for enhanced electrocatalytic methanol oxidation, Int. J. Hydrogen Energy 44 (2019) 23074–23080.

[18] D. Bokov, et al., Nanomaterial by sol-gel method: synthesis and application, Adv. Mater. Sci. Eng. (2021:) 1–21, https://doi.org/10.1155/2021/5102014.

[19] T. Huang, et al., Ultrafine Ni-B nanoparticles for efficient hydrogen evolution reaction, Chinese J. Catal 40 (2019) 1867–1873, https://doi.org/10.1016/S1872-2067(19)63331-0.

[20] D.W. Baudrand, Electroless nickel plating. ASM Handbook, vol. 5, 1994, pp. 290–305.

[21] H. Li, H.X. Li, J.F. Deng, The crystallization process of ultrafine Ni–B amorphous alloy Deng, Mater. Lett. 50 (2001) 41–46.

[22] S. Pal, N. Verma, V. Jayaram, S.K. Biswas, Y. Riddle, Characterization of phase transformation behaviour and microstructural development of electroless Ni–B coating, Mater. Sci. Eng. A 528 (28) (2011) 8269–8276.

[23] K.L. Gilley, et al., Heat treatments modify the tribological properties of nickel-boron coatings, ACS Appl. Mater. Interfaces 4 (6) (2012) 3069–3076.